Band Theory: Origin of Energy Bands

Energy bands exist in solids because of **Pauli's exclusion principle**: in an isolated atom, electrons occupy discrete energy levels. When atoms get closer to each other to form a crystal or a solid, their electrons cannot occupy the same levels of energy, as shown in the diagram.

In a **covalent union** between two atoms, Pauli's exclusion principle would be violated if two electrons were occupying the same energy levels of both atoms when isolated. All electrons thus occupy two discrete, separate levels, starting from lower energies.

When the number of atoms increases, the two levels are subdivided into other **discrete energy levels** very close to each other, forming occupied and unoccupied energy bands, as well as forbidden bandgaps. The bandgaps depend on the lattice constant; a lower-energy band is called a **valence band** (VB), and a greater-energy band is called a **conduction band** (CB).

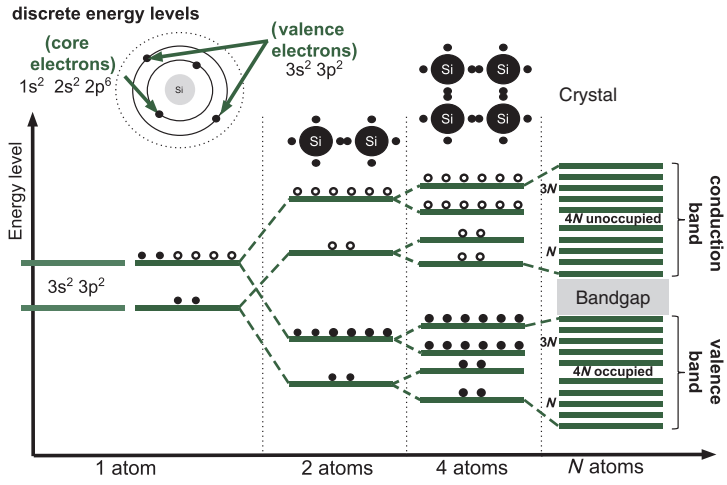

Fermi–Dirac Distribution Function

In a solid, electrons and holes—like any indiscernible particle with a half-integer spin (called ½ spin fermions)—obey **Fermi–Dirac statistics**. In a system where a large number of charge carriers fill discrete energy levels complying with Pauli's exclusion principle, Fermi–Dirac statistics are used to describe the distribution of these particles over the energy states. The distribution is given by

$$f_n(E) = \frac{1}{1 + \exp\left[\frac{E - E_F}{k_B T}\right]}$$

As shown in the plot, $f_n(E)$ has a strong dependence on temperature T, and an increase in this parameter, related to higher kinetic energy in the system, will enable a larger number of electrons to reach levels above the Fermi level E_F.

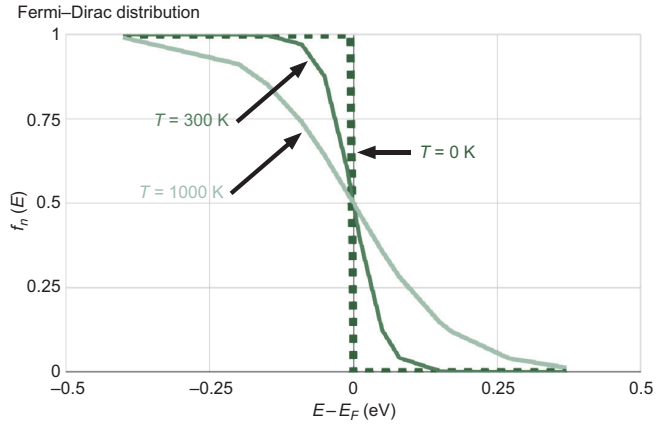

Continuity Equations for Carriers

Once the charge carrier distributions and all relevant transport processes (conduction, diffusion, generation, and recombination) have been defined, it is possible to write **continuity equations** for both types of carriers. These equations govern the general conditions of **dynamic equilibrium** and are written as

$$\frac{\partial n}{\partial t} = n\mu_n \frac{\partial E}{\partial x} + \mu_n E \frac{\partial n}{\partial x} + D_n \frac{\partial^2 n}{\partial x^2} + g_n - r_n$$

$$\frac{\partial p}{\partial t} = \underbrace{-p\mu_p \frac{\partial E}{\partial x} - \mu_p E \frac{\partial p}{\partial x}}_{\text{Drift}} + \underbrace{D_p \frac{\partial^2 p}{\partial x^2}}_{\text{Diffusion}} + g_p - r_p$$

These equations describe all phenomena perturbing the unbound carriers of a semiconductor material. The first two terms define the drift process of the carriers under the influence of an electric field **E** for electrons n and holes p. The remaining terms describe the diffusion process and account for the generation (g_n, g_p) and the recombination (r_n, r_p) rates.

Physically, as illustrated below, these differential equations essentially depict the time variation of the carrier densities due to the difference between the incoming and outgoing flux of free carriers ($J = J_c + J_d$, where $J_c = J_{cond}$, and $J_d = J_{diff}$) in the material, considering also a possible generation and recombination.

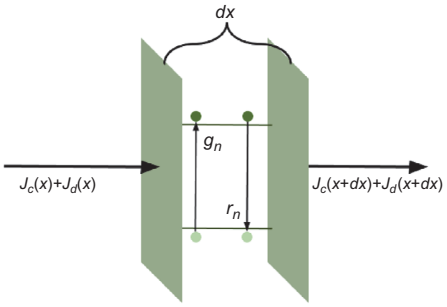

I-V Characteristics

The **total current density** J_D is expressed as a function of the bias forward voltage V by the following equation:

$$J_D = J_{s0}\left[\exp\left(\frac{eV}{kT}\right) - 1\right]$$

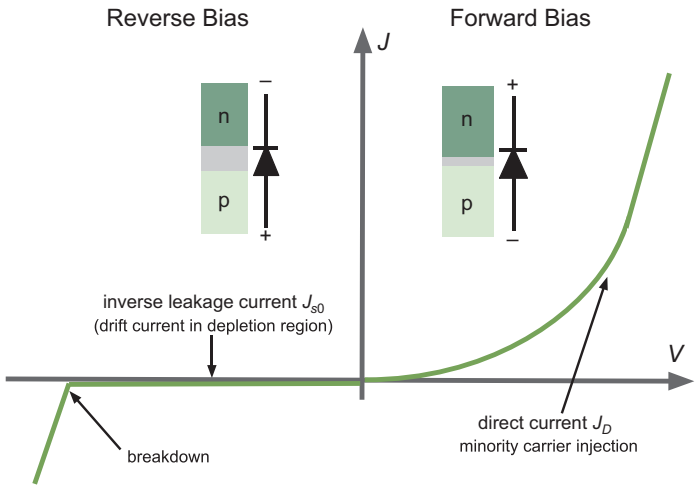

When defining the **saturation current** J_{s0} in detail, it becomes clear that this current depends on the semiconductor material used to build the diode and is usually expressed as a function of the bandgap-dependent potential $V_g = \frac{E_g}{e}$. This leads to

$$J = J_0 \exp\left[\frac{e(V - V_g)}{kT}\right]$$

Scales in MIE and Rayleigh Scattering

The effects of **elastic scattering** depend on the **size of the scatterer** (e.g., a **particle**) relative to the **wavelength** of light. For a particle radius much smaller than the wavelength ($r < \lambda/10$), scattering is known as **Rayleigh scattering**. At larger scales, the scattering is described by **Mie scattering** theory ($r > \lambda/10$). As shown in the figure, light can be scattered in all directions.

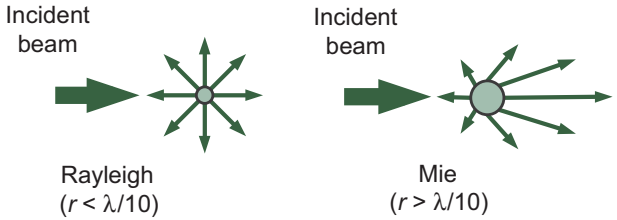

Rayleigh scattering arises due to small particles such as atoms or molecules, and photons are scattered in all directions **uniformly**. This effect varies inversely with wavelength ($\sim\lambda^{-4}$) and is therefore more noticeable at shorter wavelengths. A typical example of Rayleigh scattering is observed in the atmosphere: sunlight is scattered by **atmospheric particles**, resulting in the seemingly blue tones in the sky.

Interaction of light with larger particles leads to Mie scattering effects, which are not strongly wavelength dependent. Photons are not scattered uniformly, showing a dependence on the **angle of incidence** of light. This angle dependency becomes stronger as the size of the particle increases. Examples of Mie scattering effects can be observed from light scattered by clouds or fog, which results in a seemingly white tone.

Diffractive Elements in Waveguides

Diffraction gratings in planar waveguides are used as **light-coupling devices**. Such a grating is realized by introducing **periodic corrugations** on the surface of the waveguide (surface relief gratings), or by **periodically modulating** its **refractive index**. Because the grating modulates the phase of the incoming wave, light can be coupled into (or out of) the waveguide. Light coupling among propagating modes is also possible.

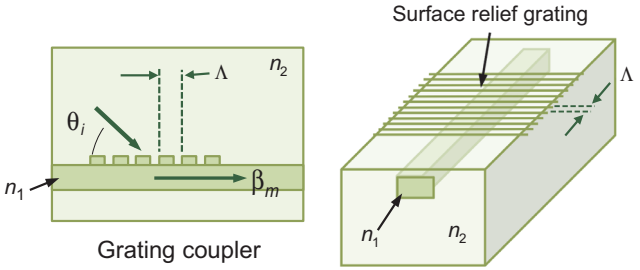

As illustrated in the figure, **grating couplers** allow for matching the phase of an incident beam (incident angle θ_i) with the propagation constant of a guided mode (β_m). The **phase-matching condition** is given by

$$\beta_m = n_2 k_0 \cos(\theta_i) + \frac{2\pi q}{\Lambda}$$

where k_0 is the wavenumber, q is the **diffraction order** (an integer), and Λ is the grating period.

Light propagating within the waveguide can be coupled to a **backward-propagating mode** upon interaction with a grating. This interacting structure is known as a **Bragg grating** and reflects light at wavelengths satisfying the condition $\lambda_B = 2\Lambda/q$. Bragg reflectors are commonly used to provide feedback in **semiconductor laser diodes**, yielding DBR (distributed Bragg reflector) or DFB (distributed feedback) laser devices. Such structures can deliver **single-mode laser operation**.

Light-Emitting Diodes (LEDs)

The basic structure of a **light-emitting diode** (LED) is a **p–n junction** of a direct-bandgap semiconductor in a **forward-bias** configuration. As shown in the band energy diagram, the injection of minority carriers creates three emitting regions: W, L_n, and L_p. Since the **injection rate** of the n^+ region is greater than that of the p region, the p-doped region presents a greater **recombination rate** and thus a higher emission. This is usually the emitting side of a LED.

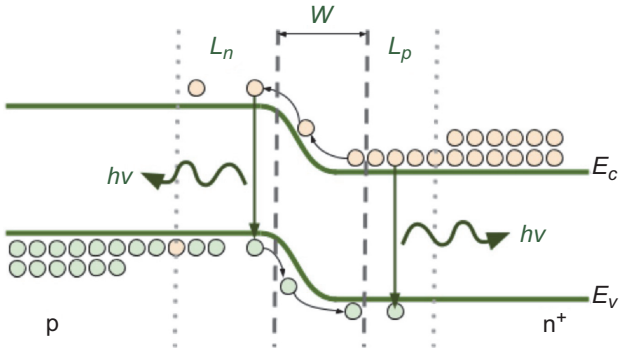

The LED optical output power P_{out} is given as a function of the **photon energy** $h\nu$, the **external quantum efficiency** η_{ext}, its cross-sectional area A, the radiative lifetime τ_r, and the excess minority carrier $n - n_0$:

$$P_{out} = \eta_{ext} h\nu A \int \frac{n - n_0}{\tau_r} dx$$

In general, LEDs show low external efficiencies due to total internal reflection: the high **refractive-index mismatch** between semiconductors (~3.5) and air causes a low-TIR angle. This must be corrected with different approaches such as **index gradients**, rough surfaces instead of flat surfaces, or even dome-shaped packaging.

Solar Cells

Solar cells are **semiconductor devices** that convert the energy of light into electricity, using the **photovoltaic effect** (PV). A PV cell or solar cell is based on a photodiode with or without external bias, and the **total electrical current** I [A/cm^2] generated by the PV cell is given by

$$I = I_{ph} - I_s\left[\exp\frac{q(V + R_s I)}{\eta kT} - 1 - \frac{V + R_s I}{R_{sh}}\right]$$

where I_{ph} is the photogenerated current due to light absorption, I_s is the reverse saturation current, η is the ideality factor (caused by undesired **recombinations** inside the device), k is Boltzmann's constant, q is the charge of the electron, R_s is the parasitic series, R_{sh} is the shunt resistance, and T is the temperature of the cell. The representation of a typical I-V curve of a solar cell is shown on the following page.

A **solar cell** can be represented by an electrically equivalent circuit model using simple discrete elements, as depicted in the diagram below. A solar cell biased by a voltage V is thus represented by a current source I_{ph} in parallel with a diode and a shunt resistance R_{sh} that, together with a series resistance R_s, account for the fact that the solar cell is not ideal.

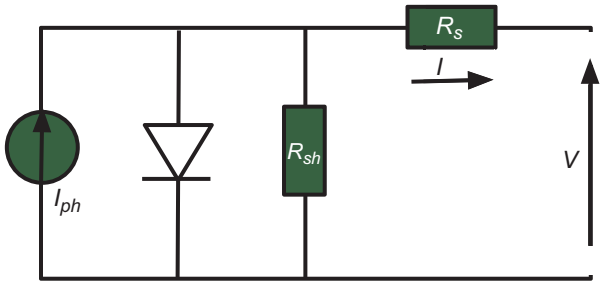

Raman Spectroscopy

Raman spectroscopy is another analytical tool to analyze materials using light in a non-invasive fashion. It is based on **Raman scattering**, in which a very small amount of light is scattered by matter following an inelastic process. (Raman scattering is represented in only about 1 out of 10^7 scattered photons coming from elastic Rayleigh-scattered light!)

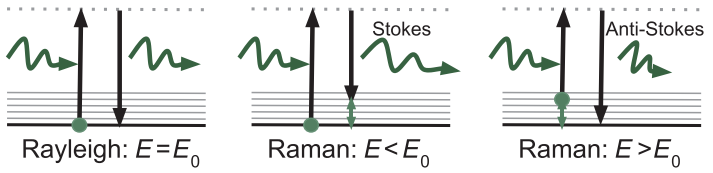

As Raman scattering is caused by a **nonresonant inelastic process**, the energy of Raman-scattered light differs from that of the incident light E_0. The energy can be either lower (Stokes Raman scattering) or greater (anti-Stokes Raman scattering) than that of E_0. Practically speaking, because the intensity of Raman scattering is very weak, Rayleigh-scattered light must be filtered using Raman spectroscopy, and only Stokes Raman-scattered photons are registered (i.e., they have greater wavelengths than the excitation wavelength).

For simplicity, only the energy/wavelength difference is considered for the **Raman spectrum**. This difference is therefore represented as the intensity of the scattered light versus the wavenumber (called the **Raman shift**). For example, the Raman peak at 547.14 nm of ethanol is obtained by a 532-nm excitation wavelength and is represented by the wavenumber 520 cm^{-1}.

Raman spectroscopy relies on a material's ability to scatter light in an **inelastic** manner. The position of a Raman-scattered intensity peak identifies a particular molecular structure. The scattering intensity is related to the substance concentration, the width of the intensity peak indicates the **crystallinity** of the material, and a shift in this peak is a sign of stress.

Equation Summary

Maxwell's equations:

For a medium with free charge density ρ_V:

Maxwell–Gauss: $\nabla \cdot \mathbf{D} = \rho_V$, or div $\mathbf{D} = \rho_V$

Maxwell's magnetic flux: $\nabla \cdot \mathbf{B} = 0$, or div $\mathbf{B} = 0$

Maxwell–Ampère:

$$\nabla \times \mathbf{H} = \mathbf{J}_f + \frac{\partial \mathbf{D}}{\partial t}, \text{ or rot } \mathbf{H} = \mathbf{J}_f + \frac{\partial \mathbf{D}}{\partial t}$$

Maxwell–Faraday: $\nabla \times \mathbf{E} = -\frac{\partial \mathbf{B}}{\partial t}$, or rot $\mathbf{E} = -\frac{\partial \mathbf{B}}{\partial t}$

Electric flux density: $\mathbf{D} = \varepsilon_0 \mathbf{E} + \mathbf{P}$

Magnetic flux density: $\mathbf{B} = \mu_0(\mathbf{H} + \mathbf{M})$

where the vector fields $\mathbf{P}$ and $\mathbf{M}$ are the polarization density and the magnetization density, respectively, of the medium.

Wave equation (D'Alambert):

$$\nabla^2 \mathbf{E} - \mu_0 \varepsilon_0 \frac{\partial^2 \mathbf{E}}{\partial t^2} = 0$$

(The same form is obtained for the magnetic field.)

Lorentz's force law:

$$\mathbf{F}_L = q(\mathbf{E} + \mathbf{v} \times \mathbf{B})$$

Varshni relation:

$$E_g(T) = E_g(0\ K) - \frac{\alpha T^2}{T + \beta} \text{ (α and β are constants)}$$

Fermi–Dirac distribution:

$$f_n(E) = \frac{1}{1 + \exp\left[\frac{E - E_F}{k_B T}\right]}$$

Equation Summary

Fiber gratings:

Bragg gratings (peak reflectivity):

$$\lambda_B = 2n_{eff}\Lambda$$

Long-period gratings (phase-matching condition):

$$\lambda_i = (n_{01} - n_{cl}{}^{(i)})\Lambda$$

Surface plasmon resonance (SPR) sensors:

$$\text{SPR angle}: \ \varphi_{\text{SPR}} = \sin^{-1}\left(\frac{1}{n_p}\sqrt{\frac{n_e^2\ n_g^2}{n_e^2 + n_g^2}}\right)$$

Laser micromachining:

Laser ablation threshold: $I_{th} = I_0 \exp\left(\frac{-2G_w^2}{d_b^2}\right)$

Juan A. Hernández-Cordero received his B.Sc. degree in electrical engineering from the Universidad Nacional Autónoma de México (UNAM). He earned Master's and Ph.D. degrees from the Division of Engineering at Brown University and spent a year as a Postdoctoral Research Associate at the Laboratory for Lightwave Technology at Boston University. He is currently a fulltime tenured researcher at the Materials Research Institute (IIM) of the UNAM, where he has established the Laboratory for Photonic Devices and Optical Fiber Sensors. Since 2001, he has lectured in Optoelectronics, Photonics, and Optical Waveguides in undergraduate and graduate programs in physics and electrical engineering at the UNAM. His fields of interest include optical fiber sensors, fiber lasers, and photonic devices for biomedical applications.

Mathieu Hautefeuille is a Professor in the Physics Department of the School of Science at Universidad Nacional Autónoma de México (UNAM), México. He received his B.Eng.Sc. and M.Eng.Sc. in Electronic Engineering from the Institut Polytechnique de Grenoble, France and his Ph.D. in Microelectronics Engineering from University College Cork, Ireland. He lectured on Optoelectronics and Electronic Instrumentation & Measurements, as well as the Physics of Semiconductors and Interaction of Radiation–Matter between 2011 and 2020 and has focused on applying these topics in his research on laser microfabrication of biomaterials, biosensors development, and imaging. He was responsible for the LaNSBioDyT National Lab at UNAM between 2015 and 2020 and has contributed more than 40 articles to international journals.